

A method for polyclonal antigen-specific T cell-targeted genome editing (TarGET) for adoptive cell transfer applications

Darya Palianina,^{1,5} Raphaël B. Di Roberto,^{2,5} Rocío Castellanos-Rueda,^{2,3} Fabrice Schlatter,² Sai T. Reddy,² and Nina Khanna^{1,4}

¹Department of Biomedicine, University and University Hospital of Basel, 4056 Basel, Switzerland; ²Department of Biosystems Science and Engineering, ETH Zürich, 4058 Basel, Switzerland; ³Life Science Zurich Graduate School, Systems Biology, ETH Zürich, University of Zurich, 8057 Zürich, Switzerland; ⁴Division of Infectious Diseases and Hospital Epidemiology, University Hospital of Basel, 4031 Basel, Switzerland

Adoptive cell therapy of donor-derived, antigen-specific T cells expressing native T cell receptors (TCRs) is a powerful strategy to fight viral infections in immunocompromised patients. Determining the fate of T cells following patient infusion hinges on the ability to track them *in vivo*. While this is possible by genetic labeling of parent cells, the applicability of this approach has been limited by the non-specificity of the edited T cells. Here, we devised a method for CRISPR-targeted genome integration of a barcoded gene into Epstein-Barr virus-antigen-stimulated T cells and demonstrated its use for exclusively identifying expanded virus-specific cell lineages. Our method facilitated the enrichment of antigen-specific T cells, which then mediated improved cytotoxicity against Epstein-Barr virus-transformed target cells. Single-cell and deep sequencing for lineage tracing revealed the expansion profile of specific T cell clones and their corresponding gene expression signature. This approach has the potential to enhance the traceability and the monitoring capabilities during immunotherapeutic T cell regimens.

INTRODUCTION

Adoptive cell transfer of donor-derived antigen-specific T cells expressing native T cell receptors (TCRs) with defined specificities is an attractive immunotherapy strategy for clinical indications where polyclonality is beneficial.¹ T cell therapies against cancer based on engineered TCRs or chimeric antigen receptors (CARs) typically only target a single antigen, reducing their applicable scope and making them vulnerable to relapses via antigen escape.² In contrast, a polyclonal and polyspecific T cell population can target multiple antigens, potentially enhancing the overall effectiveness of an adoptive cell therapy.^{3,4} The feasibility of this strategy has been demonstrated with virus-specific polyclonal T cells enriched from seropositive donors via stimulation with genetically modified or Epstein-Barr virus (EBV)-transformed antigen-presenting cells (e.g., lymphoblastoid cell lines, or LCLs)⁵ or rapidly expanded from peripheral blood mononuclear cells (PBMCs) using peptide pools as stimuli.^{4,6} In this approach, single-cell antigen specificity and phenotype character-

ization can be assessed prior to transfer through methods such as flow cytometry, ELISPOT, and TCR RNA or transcriptome sequencing. These assessments become especially important during treatment. Beyond monitoring needs, the ability to identify the most therapeutically relevant clones and phenotypes is of significant interest, particularly for long-term efficacy. Recently, it was shown that CAR T cells can persist in patients as many as 10 years after infusion.⁷ While CAR T cells are readily identifiable, non-engineered therapeutic T cells are difficult to distinguish from naive T cells. Genome-based lineage tracing of adoptively transferred lymphocytes has been proposed for facilitating follow-up studies.^{8,9} For example, LCL-stimulated EBV-specific cells transduced with the *neo*-containing G1Na vector could be traced up to 9 years after adoptive transfer.^{10,11} However, the use of retroviral vectors is associated with safety risks¹² due to the largely random nature of vector integration into the genome. Targeted gene editing by CRISPR-Cas9 is a superior approach and has been successfully used to knock out genes connected to exhaustion and checkpoint inhibition (e.g., PD-1)¹³ or resist administered immunosuppressants (e.g., tacrolimus).¹⁴ However, this approach has limitations, particularly for integrating a gene of interest, known as homology-directed repair (HDR). HDR is cell-cycle dependent and restricted to actively dividing cells.¹⁵ To date, CRISPR-based HDR approaches in T cells have relied on strong and nonspecific activation through anti-CD3 antibodies or coated beads. This approach is not compatible with a polyclonal T cell therapy where only target-specific cells are desired.

Here, we describe a novel approach for targeted CRISPR-Cas9-based genome editing and lineage tracing of virus-specific T cells. Notably, our approach combines autologous peptide presentation for T cell stimulation and editing, as well as the use of a barcoded GFP cassette

Received 1 December 2022; accepted 15 June 2023;
<https://doi.org/10.1016/j.omtm.2023.06.007>

⁵These authors contributed equally

Correspondence: Nina Khanna, Department of Biomedicine, University and University Hospital of Basel, 4056 Basel, Switzerland.

E-mail: nina.khanna@usb.ch



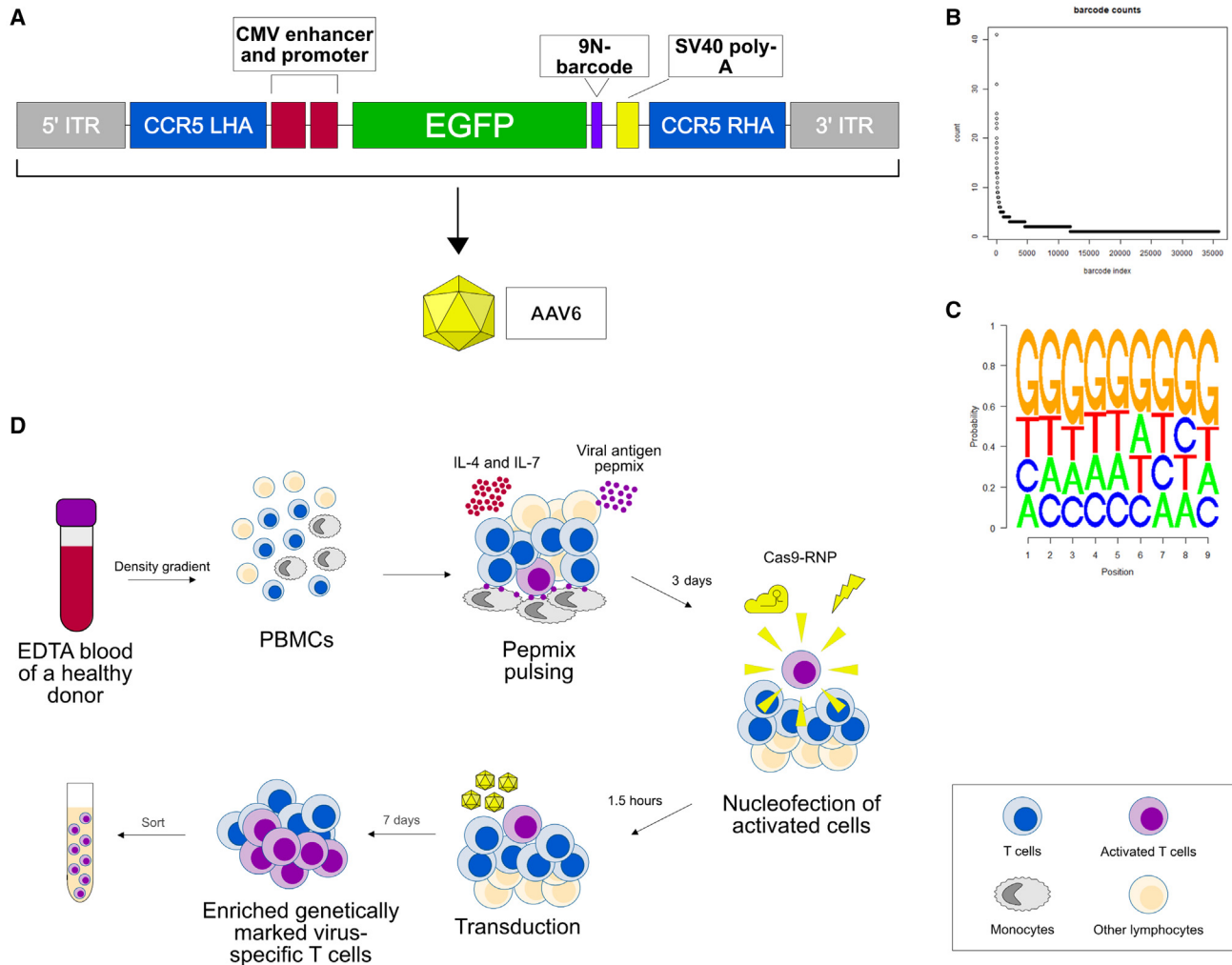


Figure 1. Library cloning and genome editing procedure

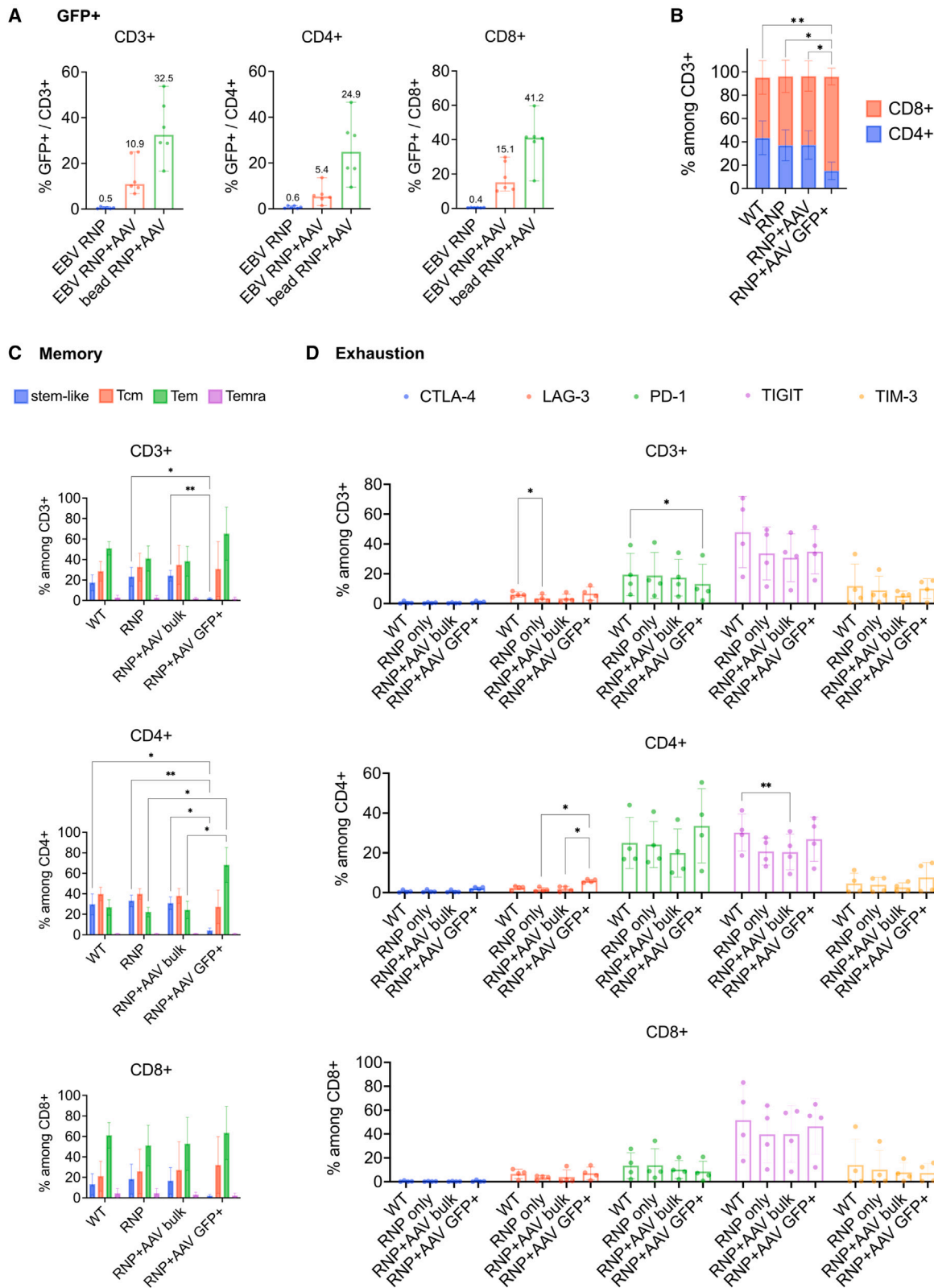
(A) Library vector and repair template DNA design. Next-generation sequencing (NGS) library analysis: (B) sequencing visualization and (C) sequence logo plots of the cloned library. (D) Schematic of the cell culture and gene editing procedures. ITR, inverted terminal repeat; LHA and RHA, left and right homology arms, respectively; CCR5, C-C chemokine receptor type 5; CMV, cytomegalovirus; SV40 polyA, simian vacuolating virus 40 polyadenylation signal; AAV6, adeno-associated virus serotype 6; EDTA, ethylenediaminetetraacetic acid; PBMCs, peripheral blood mononuclear cells; RNP, ribonuclear protein.

library to enable the detailed characterization of clonal expansion. Using antigen-presenting cells and T cells directly from donor-derived PBMCs, we generated a pool of uniquely barcoded EBV-specific T cells. By leveraging the cell-cycle dependence of HDR, we used GFP integration as a marker of EBV specificity for enrichment by fluorescence-activated sorting (FACS). Sorted GFP-positive populations were devoid of unreactive cells as shown by single-cell RNA sequencing. This high purity resulted in an increased EBV specificity and cytotoxicity against target cells (EBV-LCLs). Our method has a range of scientific and clinical applications: e.g., the possibility for sophisticated follow-up after adoptive transfer on a single cell level, lineage tracing, and the specific integration of therapy-enhancing genes such as a safety switch¹⁶ or cytokines.¹⁷

RESULTS

Library design and peptide-based T cell expansion

In order to fluorescently label and barcode specific T cells in a single step, we designed an adeno-associated virus (AAV) vector encoding (1) inverted terminal repeats (ITRs); (2) homology arms for targeted insertion into the *CCR5* gene, a popular safe harbor site for genomic integration, especially in the context of immunotherapy¹⁸; (3) the cytomegalovirus (CMV) constitutive promoter; (4) the GFP open reading frame (ORF); and 5) a 9-nucleotide barcode (Figure 1A). Although the diversity of our library could theoretically encompass 262,144 unique barcodes, we restricted its size by collecting an estimated 50,000 colony-forming units. Sequencing of this cloned library identified 36,030 unique barcodes (Figure 1B) and no major



(legend on next page)

bias (Figure 1C). The repair template library was packaged into AAV6 capsid commercially and subsequently used for HDR following transfection.

To expand EBV-specific T cells from human PBMCs, we adapted an established protocol for rapid expansion of virus-specific cytotoxic T cells (CTLs)^{19–21} and used the PepTivator EBV Consensus peptide pool as stimulus for display by native monocytes.⁴ This mixture covers 41 lytic and latent EBV antigens. It was previously shown that HDR is generally restricted to the S/G2 phases of the cell.²² Thus, proliferative activated T cells will preferentially undergo HDR following genome editing. We hypothesized that a population of pepmix-activated virus-specific T cells could be selected on the basis of successful HDR editing. To identify the optimal time point for gene editing, we characterized the T cell proliferation and activation profiles of PBMCs from two healthy EBV-seropositive donors with whole-cell staining and intracellular cytokine staining (ICC) every second day following EBV pepmix restimulation. No proliferation was observed among bulk T cells (Figure S1A) and EBV-responsive T cells (Figure S1B) by day 3, while daughter cells were present at day 5 and an abundant fraction of these were EBV-specific T cells. This lag between stimulation and expansion provided us with an opportune window for genome editing. By transfecting and transducing prior to exponential cell expansion, we aimed to edit as many parent cells as possible. As such, we opted to introduce our barcoded library during this lag time, i.e., on day 3.

Efficient transduction of peptide-stimulated T cells

In order to induce the genomic integration of a library in EBV-specific T cells, we devised the following strategy (Figure 1D). Following PBMC isolation from a healthy donor, cells were pulsed with EBV pepmix or stimulated with anti-CD3/CD28 dynabeads in the presence of interleukin (IL)-4/IL-7. On day 3, cells were transfected with CRISPR-Cas9 ribonucleoprotein (RNP) and transduced with AAV6 particles carrying the barcoded GFP library. An RNP-only sample was included to serve as an HDR-negative control. On day 10, we analyzed cell type counts as well as GFP positivity. All samples including AAV-transduced were highly CD3+ enriched, confirming the efficiency of the pepmix and cytokine conditions for T cell enrichment (Figure S2). Cells transduced with the library showed GFP expression in both pepmix-stimulated and CD3/CD28 dynabeads-stimulated cells (Figure 2A). Integration efficiency was donor-specific, ranging from 6.8% up to 25.0% for pepmix-stimulated cells and from 16.6% to 53.8% for bead-stimulated ones. For pepmix-stimulated product, we observed a higher proportion of GFP-positive T cells within the CD8+ population (median 15.1%) compared with

those within the CD4+ one (median 5.4%), and we observed a similar trend for bead-activated T cells (medians 41.2% for CD8+ and 24.9% for CD4+). We also saw enrichment of CD8+ T cells in the AAV-transduced GFP-positive EBV-activated T cells compared with the bulk-transduced ones, wild-type or RNP-transfected-only product (Figure 2B). This was most likely due to a generally higher proliferative capacity of CD8+ T cells,²³ which resulted in a higher HDR frequency within this population.²²

Next, we analyzed the memory phenotype of the generated EBV-CTLs (Figure 2C). While wild-type samples showed an even mixture of early differentiated stem-like (here defined as bulk CD45RA+ CD62L+), central memory (T_{CM} , CD45RO+ CD62L+), and effector memory T cells (T_{EM} , CD45RO+ CD62L-) with only a small minority of terminally differentiated (T_{EMRA} , CD45RA+ CD62L-) cells, we observed a depletion of the stem-like population in GFP-positive T cells, which comprised almost exclusively T_{CM} and T_{EM} . This effect could be explained by the low initial number of early differentiated (e.g., stem cell memory) EBV-CTLs in PBMCs due to EBV reactivation.²⁴ Alternatively, early differentiated EBV-specific T cells might not be activated enough to enable HDR. Generally, CD4+ cells had a less differentiated phenotype compared with CD8+ in all conditions except among those GFP+ gated. Interestingly, among CD4+ GFP+ cells, there was a significantly higher proportion of T_{EM} compared with bulk-transduced cells.

We then assessed the expression of several exhaustion markers: CTLA-4, LAG-3, PD-1, TIGIT, and TIM-3 (Figure 2D). CTLA-4 was almost absent in all conditions, LAG-3 and TIM-3 were expressed at very moderate levels. PD-1 was overall also low and decreased in AAV-transduced cells but more present in CD4+ populations (increased among AAV-transduced CD4+ cells due to a larger T_{EM} abundance). On the contrary, TIGIT was expressed at high levels in CD8+ cells but less abundant in CD4+, decreasing further with both RNP-only transfection and AAV transduction.

Together, these results indicate that the unique expansion and genome editing protocol efficiently integrated GFP in a population of activated T cells and did not markedly interfere with cell phenotype.

HDR-based sorting enriches for EBV-CTLs and improves their anti-EBV response

In order to measure the EBV specificity and activation potential of the transduced bulk and GFP-positive cells, we re-stimulated expanded cells with pepmix and analyzed the expression of key cytotoxic T cell markers such as CD107a (LAMP-1), Granzyme B, interferon

Figure 2. Transduction efficiencies and phenotype differences between expanded cells

(A) Transduction efficiencies for pepmix-stimulated vs. anti-CD3/CD28 dynabeads-stimulated T cells for bulk CD3+, CD4+, and CD8+ cells, respectively; n = 6, shown are medians with range. (B) CD4 vs. CD8 proportions within different populations of expanded pepmix-stimulated T cells; n = 6, shown are means with SD. (C) Memory phenotypes and (D) exhaustion marker expression of expanded pepmix-stimulated T cells among wild-type (WT), RNP-only transfected and transduced bulk CD3+, CD4+, and CD8+ cells; n = 4. For (B)–(D), asterisks represent statistically significant differences (*p < 0.05, **p < 0.005, two-way ANOVA, Tukey's multiple comparisons test). ANOVA, analysis of variance; EBV, Epstein-Barr virus; RNP, ribonucleoprotein; AAV, adeno-associated virus; Temra, terminally differentiated; Tem, effector memory; Tcm, central memory; Tscm, stem cell memory T cells.

A Specificity and Cytotoxicity

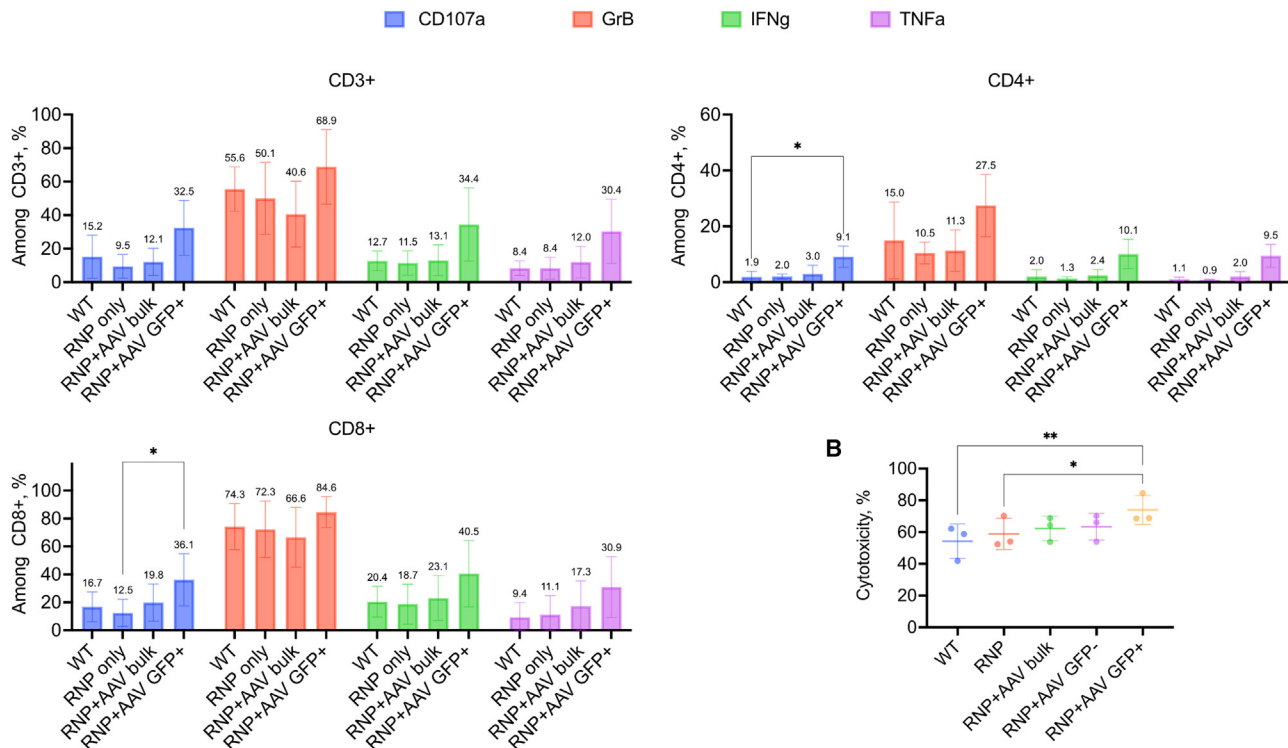


Figure 3. Specificity and functionality of pepmix-stimulated and expanded transduced T cells

(A) Production of cytotoxicity markers and cytokines (CD107a, Granzyme B, IFN γ , and TNF α) among bulk CD3+, CD4+, and CD8+ populations in response to EBV-pepmix-restimulation, $n = 4$, means with standard deviation (SD). Asterisks represent statistically significant differences ($*p < 0.05$, $**p < 0.005$, two-way ANOVA, Tukey's multiple comparisons test). (B) Six-hour cytotoxicity assay against autologous EBV-transformed LCLs (effector/target = 20:1), means of triplicates with SD for three donors, two-way ANOVA mixed effects analysis, $** = 0.0043$, $* = 0.0405$, $\alpha = 0.05$. ANOVA, analysis of variance; EBV, Epstein-Barr virus; WT, wild type; RNP, ribonucleoprotein; AAV, adeno-associated virus; GrB, granzyme B.

(IFN) γ and tumor necrosis factor (TNF) α using flow cytometry. While RNP-only transfected and bulk AAV-transduced cells did not show elevated cytotoxic marker expression compared with wild-type, within the GFP-positive T cell populations we saw elevated production of most markers (CD107a, IFN γ , and TNF α) corresponding to at least a 2-fold increase in EBV specificity for CD8+ cells and 4-fold for CD4+ cells compared with wild-type (Figure 3A).

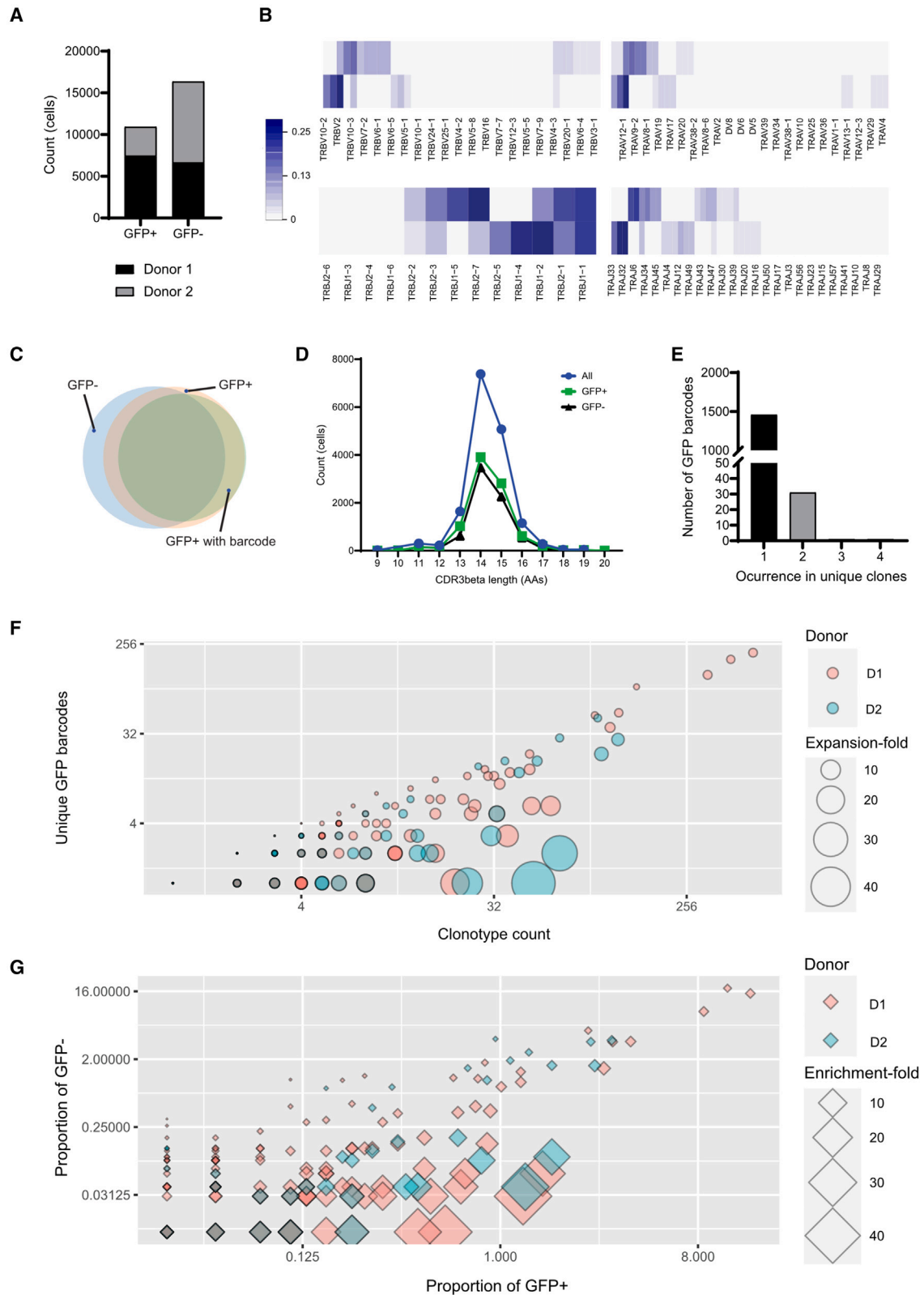
To assess target-specific functionality, we sorted GFP-positive and GFP-negative fractions of transduced EBV-CTLs and assessed their *in vitro* cytotoxicity against autologous EBV-transformed LCL and compared it with that of the other samples (Figure 3B). Although we observed a slight increase of cytotoxicity in the RNP-only samples as well as the GFP-negative sorted fractions, this was less significant than that of the sorted GFP-positive cells highlighting the efficacy-enhancing potential of HDR-based selection.

These findings show that the designed HDR-based selection of EBV-CTLs leads to an increased antigen specificity and target-specific toxicity.

GFP barcoding and selection provide expansion and enrichment statistics, respectively

Ten days following peptide pulsing, we sequenced 38,908 cells across two donors and the two sorting conditions (GFP-positive and GFP-negative) from which 27,283 had a properly annotated TCR (Figure 4A). Single-cell sequencing provided us with three layers of data for both edited and unedited T cells: (1) TCR clonal identity; (2) GFP barcode clonal identity; and (3) gene expression (transcriptome) profiles. Among all cells, 295 unique TCR clonotypes appeared at least three times. One highly represented clonotype, representing 45% and 65% of the GFP-positive and -negative datasets for donor 2, respectively, was omitted for TCR identity analysis as a likely indiscriminately expanding clone. Of the remaining clonotypes, none were shared between donors, while V- and J-gene usage diversity was also distinct (Figure 4B).

We next compared the GFP-positive and -negative sorted samples. Clonotype overlap between samples was high (Figure 4C), while CDR3 length distribution was a close match (Figures 4D and S3A). To better distinguish between clonotypes, we investigated



(legend on next page)

post-GFP integration fold-expansion (cell proliferation after day 3) and fold-enrichment (selection efficiency). For expansion, we performed a lineage tracing analysis through amplification (Figure S4) and deep sequencing of the GFP gene to specifically link cell and GFP barcodes. We obtained GFP barcodes for 44% of the sequenced GFP-positive cells, representing 1,491 unique barcodes. Only a minor fraction of these (2%) was associated with more than one TCR clonotype (Figure 4E) and was excluded from subsequent analyses. Using the ratio of GFP barcodes to cell barcode, we calculated the mean fold-expansion of 209 individual T cell clonotypes (Figure 4F). While the highest expansion was 49-fold (with one GFP barcode), the middle 50% of clones ranged between 1- and 3-fold. Notably, high expansion of a TCR clonotype did not necessarily correspond to a high cell number count; while some clonotypes had a very high expansion-fold, these were less represented than some clonotypes that expanded less, but that had many progenitors (many barcodes). Evidence suggests expansion may be a more relevant metric vs. frequency,²⁵ and barcoding allows us to distinguish the two.

In addition to fold-expansion, we calculated fold-enrichment for the 170 clonotypes that were assigned to a GFP barcode and had cells in both GFP-negative and -positive samples, based on their enrichment across samples (Figure 4G). Selection on this basis resulted in enrichment as high as 43-fold, or in depletion as high as 12-fold. Fold-expansion and fold-enrichment showed a significant correlation ($p < 0.0001$) though perhaps driven by a handful of clonotypes (Figure S3B).

We submitted the beta chains' V-gene, J-gene, and CDR3 for TCRs with barcoded GFP to TCRex, a tool for querying TCR specificity in public databases (TCRex (biodatamining.be)). Fourteen clones within 11 clonotypes were classified as EBV-specific, three of which showed enrichment and expansion both above one (Table 1). Of these, two are perfect matches by CDR3 β to dominant clones highlighted in previous work,^{26–28} while clonotype 110 is a close match (Levenshtein distance of 3). EPLPQGQLTAY and GLCTLVAML correspond to peptides from BMLF1 and BZLF1 lytic EBV proteins, while HPVGEADYFEY (EBNA1) and IVTDFSVIK (EBNA4) correspond to the latent ones. While this affirms that we identified multiple EBV-specific TCRs, the limited size of this subset speaks of the enormous diversity of TCR-epitope pairs that remains undiscovered or unrepresented even in high-quality databases.

Single-cell transcriptome sequencing confirms the enrichment of reactive T cell phenotypes in GFP-positive sorted cells

Using single-cell transcriptomics, we explored the phenotypic landscape of EBV-CTLs. Unsupervised cell clustering divided all cells into 13 main clusters (Figures 5A, 5B, and S5A–S5C). With few exceptions, CD4/CD8 identity, cell-cycle phase, cytotoxicity, and memory markers were the main drivers of cluster separation. CD8 clusters 0, 1, 2, 3, 5, 7, and 8 describe a homogeneous population of activated cytotoxic CD8 cells enriched in the expression of NKG7, GZMK, GZMA, GZMH, PRF1, HLA-DRA, and EOMES. Clustering resolves cycling cells (clusters 1 and 2), non-proliferative CD27/CCL4/CCL5-high and GZMB/LAG3-high cells (clusters 0 and 3 respectively), glycolytic cells (cluster 5), and apoptotic cells (cluster 8). Cluster 4 is a CD4-enriched cluster of moderately proliferative cells presenting an activated phenotype and retaining the expression of memory markers such as TCF7, LEF1, and CD7. CD4+ regulatory T cells (Treg) are found in cluster 9 enriched in FOXP3/ILR2A, and last, cluster 6 describes a CD4/CD8 population of resting cells enriched in memory and resting cell markers such as IL-7R, CCR7, and TCF7, which present a phenotype of unreactive T cells. Clusters 10, 11, and 12 show small populations of NK and B cells remaining from the initial whole-PBMC population.

The detection of GFP transcripts at the single-cell level was used to confirm the correct CRISPR-Cas9 genome integration of the GFP-Barcode transgene (Figures 5C and 5D). Forty-five percent of GFP-positive sorted cells had a detectable GFP transcript, compared with just 2% for the GFP-negative sample. The sub-optimal percentage for the GFP-positive cells most likely indicates sequencing subsaturation. However, it is consistent with the percentage of GFP-positive sorted cells that were assigned to a correctly annotated GFP barcode by deep sequencing (48%). Moreover, 87% of the GFP-positive sorted cells that were assigned to a correctly annotated GFP barcode also expressed GFP transcripts, confirming the accuracy of our GFP barcode readout.

When comparing the enrichment of GFP-positive and -negative cells across clusters, GFP-positive cells were strongly depleted in cluster 6 (unreactive T cells) and enriched in activated T cell clusters 1 through 5 (Figures 5C, S6A, and S6B). In addition, we saw different patterns of enrichment when looking at the expansion of TCR clonotypes within these two sample groups. Cells sorted for absence of GFP were enriched for non-expanded (only one cell per clone) and highly

Figure 4. Lineage tracing and enrichment analysis of single-cell sequencing data reveals highly expanded and highly enriched TCR clones

(A) Sequenced cell counts and their sample and donor origin. Each donor was used in a single expansion, genome editing, sorting, and sequencing workflow. Cells were sorted for the presence (GFP+) or absence (GFP-) of GFP fluorescence. (B) Heatmaps comparing the sequenced alpha and beta TCR chains and their V- and J-gene usage for each donor. Donors showed markedly different gene usage profiles. (C) Venn diagram of the membership of TCR clonotypes across GFP-positive and GFP-negative samples. The high overlap between the samples enabled the downstream calculation of enrichment statistics. (D) Distributions of the CDR3 beta lengths for GFP+ and GFP- samples. The distributions do not differentiate between samples. (E) Frequencies of identical GFP barcodes found in more than one T cell clone, based on TCR identity. The vast majority of GFP barcodes were associated with only a single clone, confirming that the barcode library was sufficient. (F and G) Scatterplots of the fold-expansion and fold-enrichment, respectively, for individual clonotypes. Fold-expansion was calculated from the ratio of GFP barcodes to clonotype count. Fold-enrichment was calculated from the ratio of proportions within libraries, from GFP- to GFP+. Gray data points show perfect overlap across donors. Both statistics enable clonotype comparisons.

Table 1. EBV-specific TCR clones within GFP-positive and barcoded dataset as predicted by TCRex

TRBV gene	CDR3 beta	TRBJ gene	Enrichment	Expansion	Epitope	TCRex score
TRBV10-03	CATGTGDSNQPQHF	TRBJ01-05	0.76	2.13	EPLPQGQLTAY	0.99
TRBV03-01	CATSTGDSNQPQHF	TRBJ01-05	1.86	1.86	EPLPQGQLTAY	0.99
TRBV14	CASSQSPGGIQYF	TRBJ02-04	1.81	1	GLCTLVAML	0.99
TRBV09	CASSARSGELFF	TRBJ02-02	0.19	2	HPVGEADYFEY	0.99
TRBV11-02	CASSWGGGSNYGYTF	TRBJ01-02	0.83	6.6	IVTDFSVIK	0.97
TRBV10-03	CAAGTGDSNQPQHF	TRBJ01-05	0.76	2.13	EPLPQGQLTAY	0.95
TRBV20-01	CSARDRGIGNTIYF	TRBJ01-03	1.21	1	GLCTLVAML	0.95
TRBV03-01	CASATGDSNQPQHF	TRBJ01-05	1.86	1.86	EPLPQGQLTAY	0.92
TRBV02	CASSASSGGYYNEQFF	TRBJ02-01	0.55	3	IVTDFSVIK	0.89
TRBV02	CASSEYAGGYYNEQFF	TRBJ02-01	0.55	3	IVTDFSVIK	0.8
TRBV07-08	CASSLGQAYEQYF	TRBJ02-07	1.65	5.1	GLCTLVAML	0.78
TRBV02	CASTQSAGGFYNEQFF	TRBJ02-01	7.24	1.6	IVTDFSVIK	0.74
TRBV10-03	CASGTGPDNSNQPQHF	TRBJ01-05	0.2	1	EPLPQGQLTAY	0.66
TRBV07-06	CASSLEPGRNEKLFF	TRBJ01-04	0.62	2.3	IVTDFSVIK	0.64

expanded (more than 200 cells per clone) clonotypes as opposed to GFP-sorted cells, which were enriched in highly expanded and also moderately expanded clonotypes (5–200 cells per clone; [Figures 5E and 5F](#)). Cluster enrichment across TCR expansion bins and the top expanded clonotypes showed that overlooking moderately expanded clonotypes restricted the diversity of T cell phenotypes ([Figures S7A and S7B](#)). On the other hand, our results showed that this could be avoided by using our targeted GFP-positive selection; while most TCR expanded clonotypes clustered around the same phenotypes, the expansion of our GFP barcode was distributed more homogeneously across activated T cell phenotypes ([Figure S8](#)).

These results illustrate how our method can be more effective in identifying highly but also moderately expanded reactive T cells across any activated phenotype for both the CD4 and CD8 compartments.

DISCUSSION

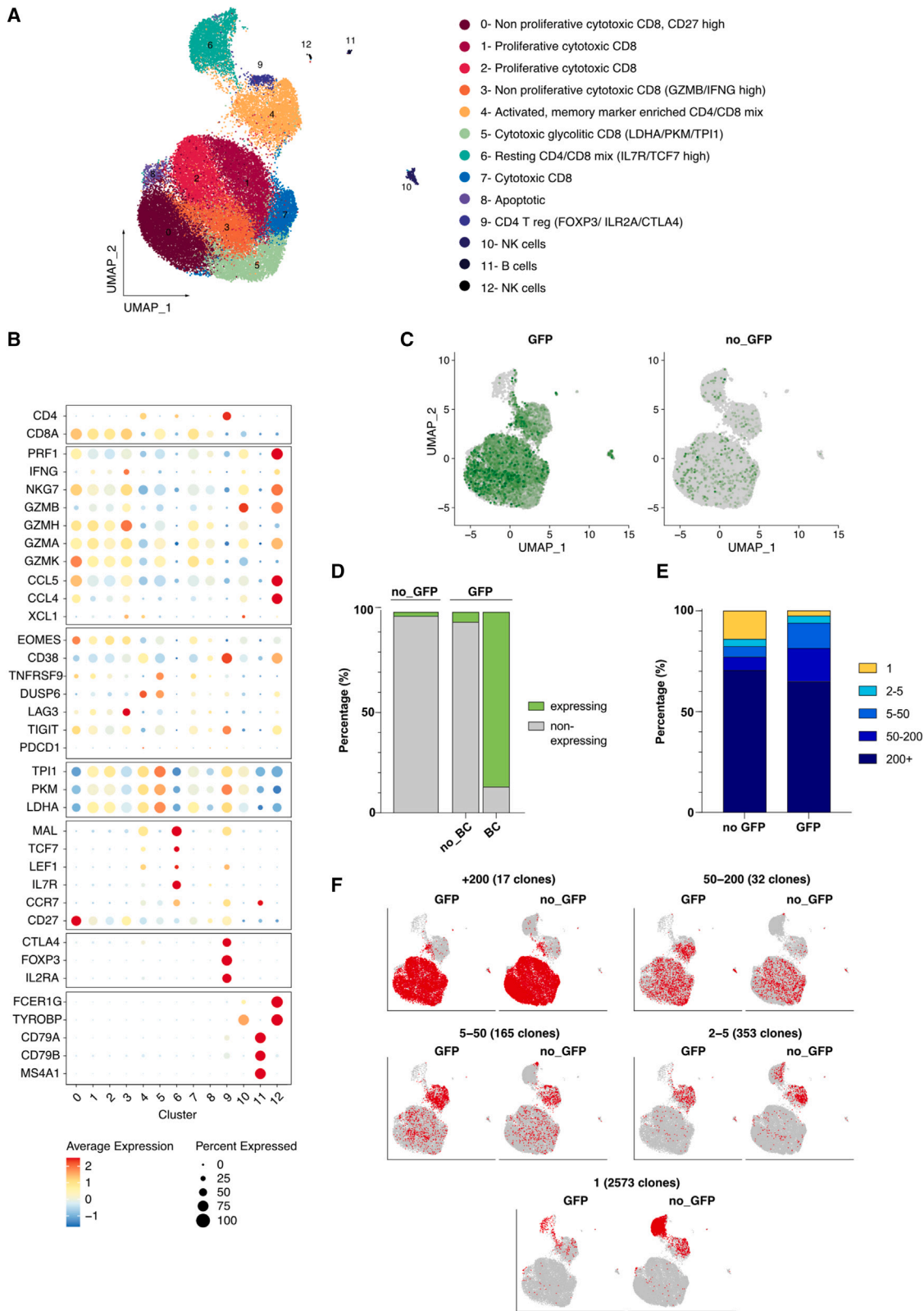
Adoptive T cell therapy is a highly versatile treatment option due to the involvement of T cell immunity in a variety of indications such as autoimmunity,²⁹ blood³⁰ and solid³¹ cancers, infectious diseases,^{32,33} and diabetes,³⁴ to name but a few. While CAR T cells are becoming a standard-of-care treatment for some hematological malignancies, patients with other challenging indications would benefit from alternative options with enhanced efficacy and persistence or with a broader targeting spectrum, such as those afforded by the use of isolated antigen-specific T cells with native TCR, as shown for virus-associated malignancies.¹⁸

Here, we present an efficient and polyvalent method of targeted gene delivery into antigen-specific T cells using a CRISPR protocol adapted to the use of peptide antigens as HDR-enabling stimuli in contrast to the commonly used nonspecific anti-CD3/CD28 stimulation of T cells. Although we focused on EBV-CTLs as a proof of concept, we note that this method does not depend on the specifics of this

model, and can therefore also be applied to other antigen targets such as anti-tumor WT1-reactive T cell enrichment for anti-leukemic activity.³⁵ Furthermore, though we employed GFP as a selection marker for FACS, our HDR approach can be used to integrate other gene expression cassettes, including immunotherapeutic enhancements such as calcineurin or FKBP12 mutants,³⁶ or inert surface markers such as truncated epidermal growth factor receptor (EGFRt)³⁷ or truncated low-affinity nerve growth factor receptor (tLNGFR).³⁸

The use of genome editing for cell engineering offers notable advantages, in particular the precision of DNA construct integration. This ensures minimal disruption of cell function when using a pre-established safe harbor site like CCR5. While CCR5 does perform an immunological function, its role in HIV infectivity has made it a common target of genome editing experiments, as people with natural homozygous CCR5 deletion show no signs of related pathology.^{18,39} Nonetheless, to account for the possible effects of CCR5 disruption, we included CCR5 deletion-only samples in our post-transduction phenotypic and functional analyses, which revealed no difference compared with wild-type. In addition to precision, genome editing ensures the long-term durability of edits, an essential feature for lineage tracing, and while a typical weakness of CRISPR-induced HDR lies in its efficiency, we were able to achieve rates of integration suitable for a substantial DNA barcode library. Coupled with the permanence of genome editing, DNA barcodes may soon become standard procedure in cell therapies,⁴⁰ making next-generation sequencers a likely soon-to-be essential tool in the clinic.

In order to assess the quality of the barcoded and selected EBV-CTLs, we combined our methodology with single-cell RNA sequencing (scRNA-seq), another tool that is revolutionizing cell engineering and immunotherapies.⁴¹ Single-cell barcode sequencing, coupled with TCR clonotype information, provided an unprecedented level



(legend on next page)

of detail on clonal expansion. In addition, scRNA-seq can link lineages to specific T cell phenotypes. The heterogeneity of stimulated T cell populations is essential to the development of effective immunity, and our genome editing protocol does not interfere with phenotype diversity. For instance, beyond the cytotoxic potential of CD8 T cells, it has been clearly shown that CD4+ T cells are crucial for sustaining anti-viral memory and effector functions.^{42,43} We observed that antigen-specific T cell stimulation combined with genome editing-based selection enabled the enrichment of EBV-CTLs with both CD4 and CD8 populations showing increased production of CD107a and cytotoxic molecules such as Granzyme B, IFN γ , and TNF α among GFP-positive cells. Memory composition is another critical parameter of an effective therapeutic T cell product.⁴⁴ Early differentiated memory phenotypes such as stem cell memory and central memory are superior in the sustaining long-term anti-tumor responses.^{45,46} Generally, we had high proportions of central memory population among the GFP-positive cells and a good enrichment of memory markers in the transcriptomics of the GFP-sorts. Interestingly, we observed a decrease of naïve-like/stem cell memory-like CD62L+ CD45RA+ population in contrast to bulk-transduced or wild-type cells that could be explained either by a slower activation of early differentiated cells compared with central and effector memory cells and as a result lower level of HDR, or by initially low amount of EBV-specific T cells among early differentiated cells due to a high frequency of EBV (CTL-controlled) reactivation in humans.²⁴ Functionally, we noted that GFP-positive sorted T cells exhibited enhanced antigen specificity and improved short-term cytotoxicity against autologous EBV-transformed LCLs. The abundance of central memory T cells among transduced CTLs indicates the long-term therapeutic potential of such products, although prospective experiments *in vivo* could help to study the long-term effect of the stem-like T cell depletion.

Our work constitutes the first instance of the precise introduction of a genetic marker targeting selected donor-derived antigen-specific T cells. The method and these data combined should help establish the next generation of cell therapies combining *in vitro* and *in vivo* lineage tracing and the functional enrichment of antigen-specific T cells.

MATERIALS AND METHODS

Plasmid library construction

The barcoded GFP library was encoded in a plasmid constructed in two steps. First, the pCMV-GFP and homology arms were designed *in silico* and synthesized externally (Twist Bioscience, South San Francisco, CA). Second, the GFP was barcoded using site-directed mutagenesis with oligonucleotide F1(RB203)* (Table S1) with nine degen-

erate “N” nucleotides and flanking regions homologous to the end of the GFP ORF and the start of the polyA signal. The oligonucleotide was used with primer R1(RB202)* in a NEBuilder assembly reaction (NEB). The resulting plasmid was transformed in electro-competent *E. coli* DH5 α cells, which were then grown in Luria-Bertani broth with 50 μ g/mL ampicillin. An aliquot was plated to assess the transformation efficiency.

PBMC extraction and cell culture

EDTA blood collected from adult healthy donors was used for PBMC extraction. The study was approved by the Ethical Committee of Northwestern and Central Switzerland (PB_2018-00081), and written informed consents were obtained. PBMCs were isolated as previously published.⁴⁷ All cells were cultured at 37°C, 5% CO₂.

EBV-specific T cell rapid expansion controlled was adapted from previous studies.¹⁹ Specifically, T cells were cultured in cytotoxic T cell line medium (CTLm) composed of RPMI (Gibco), 5% human serum, and 10,000 U/mL Penicillin-Streptomycin (Thermo Fisher Scientific, Waltham, MA). PBMCs were stimulated with either anti-CD3/CD28 Dynabeads (Thermo Fisher Scientific) according to the manufacturer’s instructions or with EBV pepmix (PepTivator EBV Consensus peptide pool [Miltenyi Biotec, Bergisch Gladbach, Germany]), at a final concentration of 60 pmol/peptide/mL in CTLm supplemented with 400 U/mL IL-4 and 10 ng/mL IL-7 (R&D Systems, Minneapolis, MN) for 3 days. After that, cells were washed, transfected, and transduced if applicable and cultured in CTLm with cytokines or cultured without genome editing.

EBV-transformed LCLs were generated using the B95.8 EBV strain as previously published.⁴⁸

Cell proliferation assay

A total of 1.5×10^7 PBMCs were stained with CellTrace Violet (CTV) Cell Proliferation Kit (Thermo Fisher Scientific) according to the manufacturer’s protocol, stimulated with the EBV pepmix and cultured in 6-well GRex plates (Wilson Wolf Manufacturing, New Brighton, MN) and cultured for 9 days. Every second day starting day 3 of culture, cells were gently resuspended and a fraction of cells was taken for ICC staining and cell proliferation tracing by flow cytometry.

Genome editing of EBV-specific T cells

PBMCs were genome-edited using a combination of CRISPR-Cas9 RNP and AAV particles after 3 days of culture with or without stimulation. The RNP was assembled by first duplexing the CRISPR RNA

Figure 5. Single-cell transcriptomics and TCR sequencing reveals a broader enrichment of EBV reactive T cell phenotypes in GFP-sorted cell samples

(A) UMAP embedding and unsupervised cell clustering of 38,908 EBV pulsed T cells. (B) Dot plot showing the expression of a selection of T cell marker genes across clusters found in (A). (C) Feature plots showing the distribution of GFP expression across cells from GFP-positive and GFP-negative sorted samples. (D) Enrichment of GFP-positive and GFP-negative sorted sample groups in GFP-expressing cells. GFP-positive sample group is further divided into cells that did or did not have a correctly annotated GFP barcode. (E) Enrichment of GFP-positive and GFP-negative sorted samples in TCR clonotypes that presented different degrees of expansion. TCR clonotypes were divided into five bins based on the number of sequenced cells annotated with each clonotype. (F) Projection of cells from five different TCR clonotype expansion bins on to the transcriptomic UMAP embedding. Cells from GFP-positive and GFP-negative sorted sample groups are shown in separate UMAP plots. BC, barcode.

(crRNA, sequence TGACATCAATTATTATACAT CGG)⁴⁹ and trans-activating CRISPR RNA (tracrRNA) (IDT) through co-incubation at 95°C for 5 min and cooling to room temperature. The duplexed RNA molecules were then complexed with 25 µg (153 pmol) of Cas9 protein (IDT) at room temperature for 20 min. The AAV particles were produced externally (Vigene Biosciences, Rockville, MD) by packaging the repair template DNA encoding the pCMV-barcoded GFP construct in an AAV6 capsid. From the PBMC cultures, cells in suspension were gently extracted without a detaching agent. The culture wells, which retained adherent monocytes, were gently washed and topped with serum-free CTL and set aside during the transfection procedure. Suspension cells were centrifuged to remove the culture medium and resuspended in 100 µL P3 nucleofection buffer (Lonza, Basel, Switzerland), to which 6.5 µL of RNP was mixed in. Cells were transferred to nucleocuvettes and shocked using a 4D-Nucleofector (Lonza) with protocol EO-115. Cells were then gently diluted in 600 µL of warm serum-free CTL medium. After 30 min, the transfected cells were placed in their original well after emptying them again without detaching monocytes. After 2 h of incubation, 20 µL of AAV particles at 2.25×10^{13} particles/mL (for a target MOI of 2×10^5 particles/cell) were added to the cultures. After 24 h, the cultures were diluted 1:1 with human serum-supplemented CTL medium.

FACS of GFP+ cells

Expanded EBV-stimulated and transduced T cells were sorted based on GFP fluorescence after 10 days of culture. Cells in suspension were gently extracted without a detaching agent and centrifuged to remove the culture medium. Cells were then washed in DPBS (Gibco), and sorted using an SH800 cell sorter (Sony Biotechnology, San Jose, CA) into CTL medium. For specificity and cytotoxicity analysis, cells were recovered for 3 days in CTLm supplemented with IL-4 and IL-7.

Staining for flow cytometry analysis of surface markers

Cells were stained with Zombie Aqua viability dye (Biolegend, San Diego, CA) in PBS, washed in FACS buffer, and stained with the cocktail of monoclonal antibodies for CD3-BUV395 (clone UCHT1), CD4-BUV496 (SK3), CD8-BUV805 (SK1), TIM-3-BV480 (7D3), PD1-BB700 (EH12.2H7) (all BD Biosciences, San Jose, CA); CD45RA-APC (MEM-56) (Thermo Fisher Scientific); CD45RO-Alexa Fluor 700 (UCHL1), CD62L-BV650 (SK11), CD27-BV421 (M-T271), CTLA-4-BV785 (L3D10), LAG-3-BV711 (11C3C65), and TIGIT-BV605 (A15153G) (all Biolegend).

Intracellular cytokine staining

Cells in a pure CTLm as a negative control and cells stimulated with EBV pepmix were seeded into a U-bottom 96-well plate containing pure CTLm as a negative control, or CTLm with 500x-diluted pepmix, respectively. Cross-linked costimulatory anti-CD28/CD49d monoclonal antibodies (BD Biosciences), 1 µg/mL each, and anti-CD107a-BV510 (H4A3, Biolegend) were added, and cells were incubated at 37°C, 5% CO₂ for 1 h. Next, cell transport was blocked by 10 µg/mL Brefeldin A (Sigma-Aldrich, Saint Louis, MO). Five-hour incubation was followed by intracellular staining for flow cytometry analysis.

Cells were stained for viability with Zombie UV dye (Biolegend) according to the manufacturer's instructions. Next, cells were washed with FACS buffer (2% sterile filtered fetal bovine serum and 0.1% NaN₃ in PBS); stained with surface monoclonal antibodies (all from BD Biosciences) for CD3-BUV395 (UCHT1), CD4-BUV496 (SK3), and CD8-BUV805 (SK1) in FACS buffer; washed; fixed with fixation buffer (Biolegend); washed with permeabilization buffer (Biolegend); and stained for 30 min with the cytokine antibodies for (all Biolegend): IFNγ-APC/Cy7 (B27), TNFα-PE/Cy7 (MAb11), and Granzyme B-PE/Cy5 (QA16A02).

Data from unstimulated controls for CD107a, IFNγ, and TNFα were subtracted from the data on stimulated samples during the analysis. As Granzyme B is prestored in memory cells,⁵⁰ the mean between unstimulated and stimulated samples was used in the analysis.

Cytotoxicity assay

T cells were incubated with autologous LCLs (Effector:Target = 20:1) for 5 h 30 min, stained for apoptosis with CellEvent Caspase-3/7 (Thermo Fisher Scientific), incubated for an additional 30 min, washed in PBS, stained for dead cells with Zombie Aqua (Biolegend), then stained for CD3+ and CD19+ in FACS buffer and analyzed by flow cytometry. LCLs incubated without T cells were used as a control. The analysis was performed as previously published.⁴ The formula used to define cytotoxicity was: % specific lysis = $100 - ([V_{\text{test}}/V_{\text{control}}] * 100)$,⁵¹ where V is percentage of viable cells (double-negative for ZombieAqua and CellEvent).

Flow cytometry analysis

Samples were acquired on the Aurora flow cytometer (Cytek, Fremont, CA) using SpectroFlo software (Cytek). Data were processed using FlowJo (FlowJo, Ashland, OR).

Statistical analysis of flow cytometry data

Data were analyzed in Prism (GraphPad, San Diego, CA) via whichever statistical methods were applicable.

Genomic PCR

Genomic DNA from 10⁴ to 10⁵ T cells was extracted using QuickExtract buffer (Lucigen, Hoddesdon, UK). The resulting product was used as a DNA template for a first PCR amplification reaction using primers F2(RB198)* and R2(RB199)* (Table S1). The 3-kbp product was extracted by gel agarose electrophoresis and used as template for a second PCR amplification using primers F3(RB214)* and R3(RB215)*. The final amplicons were purified and sequenced externally by Illumina paired-end sequencing (GENEWIZ).

Single-cell sequencing

Single-cell sequencing was done according to the 10x Genomics (Pleasanton, CA) pipeline and the manufacturer's instructions as previously described.⁵² Briefly, for each donor, 20,000 GFP-expressing cells and 20,000 GFP-negative cells were sorted as described above and processed for single-cell sequencing using a Chromium Next GEM Single Cell 5' Library & Gel Bead Kit v1.1, a Chromium Next

GEM Chip G Single Cell Kit, and a Chromium Controller. The gene expression (GEX) and the fragmented TCR VDJ targeted enrichment libraries were prepared using a Chromium Single Cell 5' Library Construction Kit and a Chromium Single Cell V(D)J Enrichment Kit, Human T cell. For GFP-targeted enrichment, the primers F4(RB200)* and R4(RB222)* were used in a PCR amplification reaction. The resulting product was used as a template for a second PCR amplification using an indexing primer and primer R5(RB201)*. All libraries were indexed using primers from a Chromium i7 Multiplex Kit and sequenced by the Genomics Facility Basel (Basel, Switzerland) using an Illumina Novaseq (Illumina, San Diego, CA) and a single lane of an S4 flow cell.

Analysis of scRNA-seq GEX data

The raw scRNA-seq data were aligned to the human genome (GRCh38) using Cell Ranger (10x Genomics, version 6.0.0). In the first place a custom reference human genome, incorporating the GFP gene, was created using the *mkref* function, then the *count* function was used to obtain the raw gene expression matrix. Downstream analysis was carried out using the Seurat R package (version 4.0.1). As quality control, cells presenting a low and high number of detected UMIs ($200 < n_{\text{Feature_RNA}} < 7,000$) and high percentage of mitochondrial genes (Percentage_MT < 20% of total reads) were removed. In addition, TCR genes were removed to avoid clonotype from guiding the subsequent clustering.

After QC, a total of 38,908 cells were used for downstream transcriptomic analysis. All samples were merged, normalized, and scaled using 2,000 variable features (GFP gene was removed to avoid its influence in downstream clustering analysis) while also regressing out cell-cycle scores. Dimensionality reduction was done using the *RunPCA* function and batch effect was removed by performing harmony integration. Finally, unsupervised cell clustering and differential gene expression was used to find marker genes used for cluster annotation. Results were then visualized using UMAP dimensionality reduction and *ggplot2* R package.

Paired TCR repertoire analysis

Raw TCR scRNA-seq data were aligned to the VDJ-GRCh38-alts-ensembl (5.0.0) using Cell Ranger (10x Genomics, version 3.1.0). As quality control, only cells retaining a productive alpha and a productive beta chain were used. Downstream analysis was done using the R programming language and common packages (code available upon request). Cluster definition was performed as previously described⁵² and the comparisons of V- and J-gene usage were done using the package *bcRep*.⁵³

Analysis of scRNA-seq GFP barcode data

The GFP barcodes were linked to single cells through the 10x Genomics barcode. Where two GFP barcodes were identified (likely biallelic integration), they were concatenated and treated as one. For EBV specificity, predictions using TCRex, V- and J-gene information, along with CDR3 beta sequences, were queried against all available EBV epitopes. The output was then re-linked to clonotype identity.

DATA AVAILABILITY

The raw and processed scRNA-seq data generated in this study will be deposited in the Gene Expression Omnibus under accession number GSE234778. Additional data that support the findings of this study are available from the corresponding author upon reasonable request.

SUPPLEMENTAL INFORMATION

Supplemental information can be found online at <https://doi.org/10.1016/j.omtm.2023.06.007>.

ACKNOWLEDGMENTS

We thank the Genomics Facility Basel and FACS Core facility of the Department of Biomedicine, University Hospital of Basel, for excellent support and assistance throughout this study. Acknowledgments go to the blood donors, and to Dr. Glenn Bantug for providing the EBV strain. This work was supported by the Swiss National Foundation Grant 32003B_204944 (to N.K.), NCCR Antiresist Grant No. 180541, Switzerland (to N.K.), Bangerter-Rhyner Stiftung (to N.K.), ETH Zurich Post-doctoral Fellowship, Switzerland (to R.B.D.R.), Helmut Horten Stiftung, Switzerland (to S.T.R.), and NCCR Molecular Systems Engineering, Switzerland (to S.T.R.).

AUTHOR CONTRIBUTIONS

D.P., R.B.D.R., S.T.R., and N.K. designed the study; D.P., R.B.D.R., and R.C.R. performed experiments; R.C.R., R.B.D.R., and F.S. analyzed the sequencing data. D.P., R.B.D.R., and N.K. discussed the results. D.P., R.B.D.R., and R.C.R. wrote the manuscript with input and commentaries from all authors.

DECLARATION OF INTERESTS

The authors declare no competing interests.

REFERENCES

- Abbott, R.C., Hughes-Parry, H.E., and Jenkins, M.R. (2022). To go or not to go? Biological logic gating engineered T cells. *J. Immunother. Cancer* *10* (4), e004185.
- Sterner, R.C., and Sterner, R.M. (2021). CAR-T cell therapy: current limitations and potential strategies. *Blood Cancer J.* *11* (4), 69.
- Houghtelin, A., and Bollard, C.M. (2017). Virus-Specific T Cells for the Immunocompromised Patient. *Front. Immunol.* *8*, 1272.
- Nowakowska, J., Stuehler, C., Egli, A., Battegay, M., Rauser, G., Bantug, G.R., Brander, C., Hess, C., and Khanna, N. (2015). T cells specific for different latent and lytic viral proteins efficiently control Epstein-Barr virus-transformed B cells. *Cytherapy* *17* (9), 1280–1291.
- Leen, A.M., Myers, G.D., Sili, U., Huls, M.H., Weiss, H., Leung, K.S., Carrum, G., Krance, R.A., Chang, C.C., Mollndrem, J.J., et al. (2006). Monoculture-derived T lymphocytes specific for multiple viruses expand and produce clinically relevant effects in immunocompromised individuals. *Nat. Med.* *12* (10), 1160–1166.
- Vasileiou, S., Turney, A.M., Kuvalekar, M., Mukhi, S.S., Watanabe, A., Lulla, P., Ramos, C.A., Naik, S., Vera, J.F., Tzannou, I., and Leen, A.M. (2020). Rapid generation of multivirus-specific T lymphocytes for the prevention and treatment of respiratory viral infections. *Haematologica* *105* (1), 235–243.
- Melenhorst, J.J., Chen, G.M., Wang, M., Porter, D.L., Chen, C., Collins, M.A., Gao, P., Bandyopadhyay, S., Sun, H., Zhao, Z., et al. (2022). Decade-long leukaemia remissions with persistence of CD4(+) CAR T cells. *Nature* *602*, 503–509.
- Buchholz, V.R., Schumacher, T.N.M., and Busch, D.H. (2016). T Cell Fate at the Single-Cell Level. *Annu. Rev. Immunol.* *34*, 65–92.

9. Al Khabouri, S., and Gerlach, C. (2020). T cell fate mapping and lineage tracing technologies probing clonal aspects underlying the generation of CD8 T cell subsets. *Scand. J. Immunol.* 92, e12983.
10. Heslop, H.E., Slobod, K.S., Pule, M.A., Hale, G.A., Rousseau, A., Smith, C.A., Bollard, C.M., Liu, H., Wu, M.F., Rochester, R.J., et al. (2010). Long-term outcome of EBV-specific T-cell infusions to prevent or treat EBV-related lymphoproliferative disease in transplant recipients. *Blood* 115, 925–935.
11. Rooney, C.M., Smith, C.A., Ng, C.Y., Loftin, S., Li, C., Krance, R.A., Brenner, M.K., and Heslop, H.E. (1995). Use of gene-modified virus-specific T lymphocytes to control Epstein-Barr-virus-related lymphoproliferation. *Lancet* 345, 9–13.
12. Anson, D.S. (2004). The use of retroviral vectors for gene therapy-what are the risks? A review of retroviral pathogenesis and its relevance to retroviral vector-mediated gene delivery. *Genet. Vaccines Ther.* 2, 9.
13. Zhao, Z., Shi, L., Zhang, W., Han, J., Zhang, S., Fu, Z., and Cai, J. (2018). CRISPR knock out of programmed cell death protein 1 enhances anti-tumor activity of cytotoxic T lymphocytes. *Oncotarget* 9, 5208–5215.
14. Amini, L., Wagner, D.L., Rössler, U., Zarrinrad, G., Wagner, L.F., Vollmer, T., Wendering, D.J., Kornak, U., Volk, H.D., Reinke, P., and Schmuck-Henneresse, M. (2021). CRISPR-Cas9-Edited Tacrolimus-Resistant Antiviral T Cells for Advanced Adoptive Immunotherapy in Transplant Recipients. *Mol. Ther.* 29, 32–46.
15. Karanam, K., Kafri, R., Loewer, A., and Lahav, G. (2012). Quantitative live cell imaging reveals a gradual shift between DNA repair mechanisms and a maximal use of HR in mid S phase. *Mol. Cell* 47, 320–329.
16. Gargett, T., and Brown, M.P. (2014). The inducible caspase-9 suicide gene system as a "safety switch" to limit on-target, off-tumor toxicities of chimeric antigen receptor T cells. *Front. Pharmacol.* 5, 235.
17. Pegram, H.J., Lee, J.C., Hayman, E.G., Imperato, G.H., Tedder, T.F., Sadelain, M., and Brentjens, R.J. (2012). Tumor-targeted T cells modified to secrete IL-12 eradicate systemic tumors without need for prior conditioning. *Blood* 119, 4133–4141.
18. Papapetrou, E.P., and Schambach, A. (2016). Gene Insertion Into Genomic Safe Harbors for Human Gene Therapy. *Mol. Ther.* 24, 678–684.
19. Gerdemann, U., Keirnan, J.M., Katari, U.L., Yanagisawa, R., Christin, A.S., Huye, L.E., Perna, S.K., Ennamuri, S., Gottschalk, S., Brenner, M.K., et al. (2012). Rapidly generated multivirus-specific cytotoxic T lymphocytes for the prophylaxis and treatment of viral infections. *Mol. Ther.* 20, 1622–1632.
20. Papadopoulou, A., Gerdemann, U., Katari, U.L., Tzannou, I., Liu, H., Martinez, C., Leung, K., Carrum, G., Gee, A.P., Vera, J.F., et al. (2014). Activity of broad-spectrum T cells as treatment for AdV, EBV, CMV, BKV, and HHV6 infections after HSCT. *Sci. Transl. Med.* 6, 242ra83.
21. Gerdemann, U., Katari, U.L., Papadopoulou, A., Keirnan, J.M., Craddock, J.A., Liu, H., Martinez, C.A., Kennedy-Nasser, A., Leung, K.S., Gottschalk, S.M., et al. (2013). Safety and clinical efficacy of rapidly-generated trivirus-directed T cells as treatment for adenovirus, EBV, and CMV infections after allogeneic hematopoietic stem cell transplant. *Mol. Ther.* 21, 2113–2121.
22. Cox, D.B.T., Platt, R.J., and Zhang, F. (2015). Therapeutic genome editing: prospects and challenges. *Nat. Med.* 21, 121–131.
23. Kaeck, S.M., Wherry, E.J., and Ahmed, R. (2002). Effector and memory T-cell differentiation: implications for vaccine development. *Nat. Rev. Immunol.* 2, 251–262.
24. Maurmann, S., Fricke, L., Wagner, H.J., Schlenke, P., Hennig, H., Steinhoff, J., and Jabs, W.J. (2003). Molecular parameters for precise diagnosis of asymptomatic Epstein-Barr virus reactivation in healthy carriers. *J. Clin. Microbiol.* 41, 5419–5428.
25. Neumeier, D., Yermanos, A., Agrafiotis, A., Csepreghi, L., Chowdhury, T., Ehling, R.A., Kuhn, R., Cotet, T.S., Brisset-Di Roberto, R., Di Tacchio, M., et al. (2022). Phenotypic determinism and stochasticity in antibody repertoires of clonally expanded plasma cells. *Proc. Natl. Acad. Sci. USA* 119, e2113766119.
26. Miconnet, I., Marrau, A., Farina, A., Taffé, P., Vigano, S., Harari, A., and Pantaleo, G. (2011). Large TCR diversity of virus-specific CD8 T cells provides the mechanistic basis for massive TCR renewal after antigen exposure. *J. Immunol.* 186, 7039–7049.
27. Koning, D., Costa, A.I., Hoof, I., Miles, J.J., Nanlohy, N.M., Ladell, K., Matthews, K.K., Venturi, V., Schellens, I.M.M., Borghans, J.A.M., et al. (2013). CD8+ TCR repertoire formation is guided primarily by the peptide component of the antigenic complex. *J. Immunol.* 190, 931–939.
28. Miles, J.J., Elhassen, D., Borg, N.A., Silins, S.L., Tynan, F.E., Burrows, J.M., Purcell, A.W., Kjer-Nielsen, L., Rossjohn, J., Burrows, S.R., and McCluskey, J. (2005). CTL recognition of a bulged viral peptide involves biased TCR selection. *J. Immunol.* 175, 3826–3834.
29. Baeten, P., Van Zeebroeck, L., Kleinewietfeld, M., Hellings, N., and Broux, B. (2022). Improving the Efficacy of Regulatory T Cell Therapy. *Clin. Rev. Allergy Immunol.* 62, 363–381.
30. Majzner, R.G., and Mackall, C.L. (2019). Clinical lessons learned from the first leg of the CAR T cell journey. *Nat. Med.* 25, 1341–1355.
31. Kirtane, K., Elmariam, H., Chung, C.H., and Abate-Daga, D. (2021). Adoptive cellular therapy in solid tumor malignancies: review of the literature and challenges ahead. *J. Immunother. Cancer* 9, e002723.
32. Kaeuferle, T., Krauss, R., Blaeschke, F., Willier, S., and Feuchtinger, T. (2019). Strategies of adoptive T-cell transfer to treat refractory viral infections post allogeneic stem cell transplantation. *J. Hematol. Oncol.* 12, 13.
33. Walti, C.S., Stuehler, C., Palianina, D., and Khanna, N. (2022). Immunocompromised host section: Adoptive T-cell therapy for dsDNA viruses in allogeneic hematopoietic cell transplant recipients. *Curr. Opin. Infect. Dis.* 35, 302–311.
34. Ben-Skowronek, I., Sieniawska, J., Pach, E., Wróbel, W., Skowronek, A., Tomczyk, Z., and Rosolowska, I. (2021). Potential Therapeutic Application of Regulatory T Cells in Diabetes Mellitus Type 1. *Int. J. Mol. Sci.* 23, 390.
35. Chapuis, A.G., Ragnarsson, G.B., Nguyen, H.N., Chaney, C.N., Pufnock, J.S., Schmitt, T.M., Duerkopp, N., Roberts, I.M., Pogosov, G.L., Ho, W.Y., et al. (2013). Transferred WT1-reactive CD8+ T cells can mediate antileukemic activity and persist in post-transplant patients. *Sci. Transl. Med.* 5, 174ra27. 174ra127.
36. Brevin, J., Mancao, C., Straathof, K., Karlsson, H., Samarasinghe, S., Amrolia, P.J., and Pule, M. (2009). Generation of EBV-specific cytotoxic T cells that are resistant to calcineurin inhibitors for the treatment of posttransplantation lymphoproliferative disease. *Blood* 114, 4792–4803.
37. Wang, X.J., Chang, W.C., Wong, C.W., Colcher, D., Sherman, M., Ostberg, J.R., Forman, S.J., Riddell, S.R., and Jensen, M.C. (2011). A transgene-encoded cell surface polypeptide for selection, in vivo tracking, and ablation of engineered cells. *Blood* 118, 1255–1263.
38. Bonini, C., Grez, M., Traversari, C., Ciceri, F., Marktel, S., Ferrari, G., Dinayer, M., Sadat, M., Aiuti, A., Deola, S., et al. (2003). Safety of retroviral gene marking with a truncated NGF receptor. *Nat. Med.* 9, 367–369.
39. Liu, R., Paxton, W.A., Choe, S., Ceradini, D., Martin, S.R., Horuk, R., MacDonald, M.E., Stuhlmann, H., Koup, R.A., and Landau, N.R. (1996). Homozygous defect in HIV-1 coreceptor accounts for resistance of some multiply-exposed individuals to HIV-1 infection. *Cell* 86, 367–377.
40. Masuyama, N., Mori, H., and Yachie, N. (2019). DNA barcodes evolve for high-resolution cell lineage tracing. *Curr. Opin. Chem. Biol.* 52, 63–71.
41. Castellanos-Rueda, R., Di Roberto, R.B., Schlatter, F.S., and Reddy, S.T. (2021). Leveraging Single-Cell Sequencing for Chimeric Antigen Receptor T Cell Therapies. *Trends Biotechnol.* 39, 1308–1320.
42. Pourghesari, B., Piper, K.P., McLarnon, A., Arrazi, J., Bruton, R., Clark, F., Cook, M., Mahendra, P., Craddock, C., and Moss, P.A.H. (2009). Early reconstitution of effector memory CD4+ CMV-specific T cells protects against CMV reactivation following allogeneic SCT. *Bone Marrow Transplant.* 43, 853–861.
43. Novy, P., Quigley, M., Huang, X., and Yang, Y. (2007). CD4 T cells are required for CD8 T cell survival during both primary and memory recall responses. *J. Immunol.* 179, 8243–8251.
44. Busch, D.H., Fräßle, S.P., Sommermeyer, D., Buchholz, V.R., and Riddell, S.R. (2016). Role of memory T cell subsets for adoptive immunotherapy. *Semin. Immunol.* 28, 28–34.
45. Wang, F., Cheng, F., and Zheng, F. (2022). Stem cell like memory T cells: A new paradigm in cancer immunotherapy. *Clin. Immunol.* 241, 109078.
46. Klebanoff, C.A., Gattinoni, L., Torabi-Parizi, P., Kerstann, K., Cardones, A.R., Finkelstein, S.E., Palmer, D.C., Antony, P.A., Hwang, S.T., Rosenberg, S.A., et al. (2005). Central memory self/tumor-reactive CD8+ T cells confer superior antitumor immunity compared with effector memory T cells. *Proc. Natl. Acad. Sci. USA* 102, 9571–9576.

47. Rauser, G., Einsele, H., Sinzger, C., Wernet, D., Kuntz, G., Assenmacher, M., Campbell, J.D.M., and Topp, M.S. (2004). Rapid generation of combined CMV-specific CD4+ and CD8+ T-cell lines for adoptive transfer into recipients of allogeneic stem cell transplants. *Blood* 103, 3565–3572.
48. Merlo, A., Turrini, R., Bobisse, S., Zamarchi, R., Alaggio, R., Dolcetti, R., Mautner, J., Zanovello, P., Amadori, A., and Rosato, A. (2010). Virus-specific cytotoxic CD4+ T cells for the treatment of EBV-related tumors. *J. Immunol.* 184, 5895–5902.
49. Kang, H., Minder, P., Park, M.A., Mesquitta, W.T., Torbett, B.E., and Slukvin, I.I. (2015). CCR5 Disruption in Induced Pluripotent Stem Cells Using CRISPR/Cas9 Provides Selective Resistance of Immune Cells to CCR5-tropic HIV-1 Virus. *Mol. Ther.* Nucleic Acids 4, e268.
50. Nowacki, T.M., Kuerten, S., Zhang, W., Shive, C.L., Kreher, C.R., Boehm, B.O., Lehmann, P.V., and Tary-Lehmann, M. (2007). Granzyme B production distinguishes recently activated CD8(+) memory cells from resting memory cells. *Cell. Immunol.* 247, 36–48.
51. Rubinstein, J.D., Burns, K., Absalon, M., Lutzko, C., Leemhuis, T., Chandra, S., Hanley, P.J., Keller, M.D., Davies, S.M., Nelson, A., and Grimley, M. (2020). EBV-directed viral-specific T-lymphocyte therapy for the treatment of EBV-driven lymphoma in two patients with primary immunodeficiency and DNA repair defects. *Pediatr. Blood Cancer* 67, e28126.
52. Bieberich, F., Vazquez-Lombardi, R., Yermanos, A., Ehling, R.A., Mason, D.M., Wagner, B., Kapetanovic, E., Di Roberto, R.B., Weber, C.R., Savic, M., et al. (2021). A Single-Cell Atlas of Lymphocyte Adaptive Immune Repertoires and Transcriptomes Reveals Age-Related Differences in Convalescent COVID-19 Patients. *Front. Immunol.* 12, 701085.
53. Bischof, J., and Ibrahim, S.M. (2016). bcRep: R Package for Comprehensive Analysis of B Cell Receptor Repertoire Data. *PLoS One* 11, e0161569.